Journal of Materials Chemistry A

COMMUNICATION

View Article Online
View Journal | View Issue

Cite this: J. Mater. Chem. A, 2014, 2, 3297

Received 21st November 2013
Accepted 11th December 2013

DOI: 10.1039/c3ta14818a

www.rsc.org/MaterialsA

Top-down fabrication of three-dimensional porous V_2O_5 hierarchical microplates with tunable porosity for improved lithium battery performance†

Qinyou An,‡ Pengfei Zhang,‡ Qiulong Wei, Liang He,* Fangyu Xiong, Jinzhi Sheng, Qinqin Wang and Liqiang Mai*

Three-dimensional porous V_2O_5 hierarchical microplates have been fabricated by a one-step top-down strategy, and display an excellent rate capability and stable capacity of 110 mA h g^{-1} at 2000 mA g^{-1} after 100 cycles. We have demonstrated that the facile approach of a solid-phase conversion is promising for large-scale fabrication of highly porous micro/nano materials.

Introduction

The ever increasing demand for electrochemical devices with advanced energy conversion and storage has stimulated significant interests in lithium battery (LB) research.[1–3] The lithium battery is one of the most promising energy storage systems which is efficient in delivering energy, light in weight and environmentally benign.[4–7] For applications in electric vehicles (EVs) and hybrid electric vehicles (HEVs), the energy density of LBs still needs to be improved.[7–9] Increasing the energy density of LBs requires the development of electrode materials with higher capacities.[8–12] Among the potential cathode materials, vanadium pentoxide (V_2O_5) with a layered structure has been extensively investigated due to its low cost and abundance as well as high theoretical capacity (about 294 mA h g^{-1} with 2 Li insertion/extraction per unit formula).[13–17] Even only one Li insertion/extraction, it also can deliver a comparable capacity compared to the commercialized cathode materials such as $LiCoO_2$ (140 mA h g^{-1}) and $LiMn_2O_4$ (146 mA h g^{-1}).[13,18–20] However, two critical issues for this electrode material are its low rate and limited long-term cycling stability, due to its slow electrochemical kinetics and poor structural stability.[21–23]

In the past decades, many efforts have been focused on the synthesis of micro/nano-structured vanadium oxides to mitigate against the slow electrochemical kinetics by acquiring high surface areas and short ion diffusion distances.[24] Various micro/nano-structures reported with different performances suggest that the characteristics of V_2O_5, such as its dimensions, morphology, porosity, and texture, are critically important for the electrochemical performance of the electrodes.[25–27] In particular, V_2O_5 nanostructures, such as nanowires, nanorods, nanoribbons, nanosheets and hollow structures, can effectively improve the electrochemical kinetics, shorten the diffusion distance for Li^+ ions, and buffer the volume change, maintaining mechanical integrity and chemical stability over many intercalation/deintercalation cycles as compared with non-nanostructured materials.[28–30] However, the electrochemical performance of V_2O_5 nanomaterials, particularly, the cycling stability and rate capability, is still not very satisfactory. As is well known, porous aggregates of electrode materials show great advantages such as good contact with the electrolyte, high specific surface area, improved Li^+ permeation and ease of binding compared to isolated nanosized particles, which can reduce the polarization and decrease the structure stress during the charge–discharge processes.[31–36] Furthermore, the hierarchical structures can effectively suppress the self-aggregation of electrode materials upon cycling.[36] Thus, constructing the V_2O_5 cathode material with a hierarchical porous structure has been considered to be a valid way to improve its electrochemical performance.

State Key Laboratory of Advanced Technology for Materials Synthesis and Processing, WUT-Harvard Joint Nano Key Laboratory, Wuhan University of Technology, Wuhan 430070, P.R. China. E-mail: mlq518@whut.edu.cn; hel@whut.edu.cn; Fax: +86-27-87644867; Tel: +86-27-87467595

† Electronic supplementary information (ESI) available: SEM images of the samples synthesized under different solvothermal times, EDS mapping of the porous V_2O_5 hierarchical microplate, SEM images of NH_4VO_3 microplates, TEM image of irregular V_2O_5 particle, SEM images of V_2O_5 annealed at different temperatures, nitrogen adsorption–desorption isotherms of porous V_2O_5 microplates and corresponding pore size distribution annealed at different temperatures, SEM images of NV-350, nitrogen adsorption–desorption isotherms of NV-350 and corresponding pore size distribution, SEM images and electrochemical characterizations of the bulk V_2O_5, AC-impedance spectra of V_2O_5 electrodes prepared under different calcination temperatures. See DOI: 10.1039/c3ta14818a

‡ Author contributions: Qinyou An and Pengfei Zhang contributed equally to this work. All authors discussed the results and commented on the manuscript. The authors declare no competing financial interest.

Creating an open pore-network within the bulk of the solid is an effective approach to form hierarchical porous cathode materials.[37] In this work, we report a facile top-down preparation of porous nanoarchitectures from large microcrystals. To the best of our knowledge, it may be the first time that three-dimensional (3D) porous V_2O_5 quasi-hexagonal hierarchical microplates with tunable porosity have been synthesized. When evaluated as a cathode material for LBs, the porous V_2O_5 microplates manifest significantly improved electrochemical performance in terms of specific capacity, cycling stability and rate capability.

Experimental section

Materials synthesis

In a typical synthesis, urea (1.5 g) and NH_4VO_3 (0.1 mmol) were dissolved in 10 mL deionized water in turn under vigorous stirring at 80 °C. After stirring for 20 min, 50 mL acetonitrile was added into the above solution, and then the solution continued to be stirred for 1 h. Subsequently, the mixture was transferred into a Teflon-lined stainless steel autoclave with a capacity of 100 mL. After heating at 180 °C for 12 h, the autoclave was naturally cooled to room temperature, and the precipitate was collected by centrifugation and washed three times with ethanol. Finally, 3D porous V_2O_5 hierarchical microplates were obtained by annealing the solvothermally prepared NH_4VO_3 quasi-hexagonal microplates in air at 350 °C for 2 h with a heating rate of 2 °C min^{-1}. A series of experiments were also carried out at different solvothermal reaction times and calcination temperatures to investigate the structural evolution process.

Characterization

X-ray diffraction (XRD) measurements were performed to investigate the crystallographic properties using a D8 Advance X-ray diffractometer with a non-monochromated Cu Kα X-ray source. Field emission scanning electron microscopy (FESEM) images were collected using a JEOL-7100F microscopy at an acceleration voltage of 10 kV. Transmission electron microscopy (TEM) images and high-resolution transmission electron microscopy (HRTEM) images were recorded by using a JEM-2100F STEM/EDS microscope. Brunauer–Emmet–Teller (BET) surface areas were measured using Tristar II 3020 instrument to measure the adsorption of nitrogen.

Measurement of electrochemical performance

The electrochemical properties were evaluated by assembly of 2025 coin cells in a glove box filled with pure argon gas. Lithium pellets were used as the anode, 1 M solution of $LiPF_6$ in ethylene carbon (EC)/dimethyl carbonate (DMC) was used as the electrolyte, and the cathode electrodes were obtained with 70% 3D porous V_2O_5 hierarchical microplates active material, 20% acetylene black and 10% poly (tetrafluoroethylene) (PTFE). Galvanostatic charge–discharge cycling was studied over a potential range of 2.4–4.0 V *vs.* Li/Li^+ with a multichannel battery testing system (LAND CT2001A). Cyclic voltammetry (CV) and AC-impedance spectra were tested with an electrochemical workstation (Autolab PGSTAT 302N).

Results and discussion

A schematic illustration of the synthesis of 3D porous V_2O_5 hierarchical microplates is shown in Fig. 1a. The first step of the synthesis involves the dissolution of NH_4VO_3 particles in a water bath process. The formation mechanism of NH_4VO_3 quasi-hexagonal microplates may be attributed to the anisotropic growth of their inherent crystal structure and chemical potential in solution,[38,39] which can be confirmed by the FESEM images of the products with different solvothermal reaction times (Fig. S1†). In this step, the ammonia derived from urea effectively restrains the hydrolysis of ammonium metavanadate (eqn (1)–(3)). As a result, the pure ammonium metavanadate microstructure can be obtained after the solvothermal reaction. In addition, urea shows certain ability to dissociate particles and affect the particles' aggregation through direct binding to the particles' surfaces.[40] Ultimately, the prepared NH_4VO_3 quasi-hexagonal microplates were decomposed into 3D porous V_2O_5 hierarchical microplates under an annealing process, corresponding to eqn (4).

$$NH_4VO_3 \leftrightarrow NH_4^+ + VO_3^- \quad (1)$$

$$(NH_2)_2CO + H_2O \rightarrow 2NH_3 + CO_2 \quad (2)$$

$$NH_3 + H_2O \leftrightarrow NH_4^+ + OH^- \quad (3)$$

$$2NH_4VO_3 \rightarrow 2NH_3 + V_2O_5 + H_2O \quad (4)$$

Owing to a conversion from NH_4VO_3 to its corresponding oxides, which makes use of the volume shrinkage and release of internally born ammonia (NH_3) in the process of thermal decomposition, 3D porous V_2O_5 hierarchical microplates were finally obtained. The vanadium oxide layer effectively blocking the gas release is broken by the ammonia sealed inside, forming small voids/pores. Many such processes can concurrently/continuously occur from the outer to inner part of the crystals until continuous channels are eventually formed, and NH_4VO_3 is completely decomposed to V_2O_5.[41,42]

The morphology and microstructure of the as-prepared products were examined using FESEM and TEM. The FESEM and TEM images (Fig. 1b and c) reveal that the NH_4VO_3 sample prepared by the solvothermal method is composed of quasi-hexagonal microplates with lengths of more than 10 μm. Energy dispersive spectroscopy (EDS) element mapping analysis (Fig. 1d) indicates that V, N and O are distributed in the NH_4VO_3 quasi-hexagonal microplates. Apparently, Fig. 1e, S2 and S3† show that the material morphology is essentially preserved during the annealing and solid-phase conversion process, and the porous structure can be also observed on the surface of the V_2O_5 sample calcined at 350 °C (V_2O_5-350). The representative TEM image (Fig. 1f) shows the prepared V_2O_5 quasi-hexagonal microplates are composed of interconnected nanosized

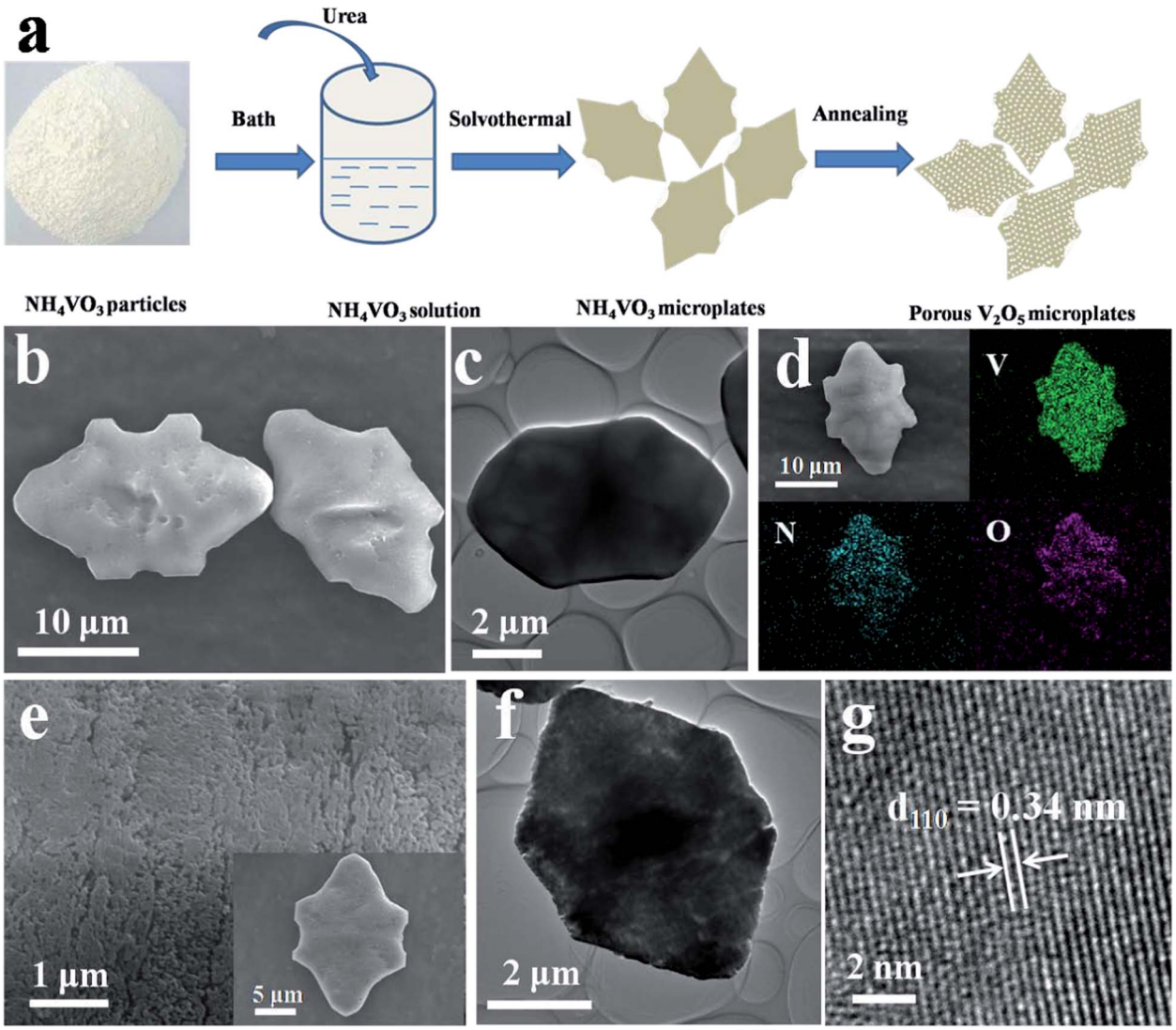

Fig. 1 (a) A schematic illustration for the formation of 3D porous V_2O_5 hierarchical microplates through the one-step thermal decomposition of NH_4VO_3 microcrystals. FESEM image (b), TEM image (c) and EDS mappings (d) of NH_4VO_3 quasi-hexagonal microplates. FESEM (e), TEM (f) and HRTEM (g) images of the 3D porous V_2O_5 hierarchical microplates annealed at 350 °C.

subunits with a highly porous structure. In the HRTEM image (Fig. 1g) taken from an edge of a nanosized subunit, the lattice fringes are clearly visible with a spacing of 0.34 nm, which is in agreement with that of the (110) planes of V_2O_5 (JCPDS card No. 00-041-1426). There are some irregular particles which can be observed in the resultant products (Fig. S4†), and their conversion to porous V_2O_5 is similar to that of the V_2O_5 quasi-hexagonal microplates (Fig. S5†).

The resultant products were characterized using XRD to identify the crystallographic structure and crystallinity (Fig. 2a). It can be observed that all of the peaks match those of orthorhombic NH_4VO_3 (JCPDS No. 00-025-0047, space group: *Pmab*, $a = 5.8270$ Å, $b = 11.7820$ Å, $c = 4.9050$ Å) and orthorhombic V_2O_5 (JCPDS No. 00-041-1426, space group: *Pmmn*, $a = 11.5160$ Å, $b = 3.5656$ Å, $c = 4.3727$ Å). The strong and narrow peaks indicate a high crystallinity of the as-prepared products. In order to confirm the phase transition, thermogravimetric (TG) analysis of the NH_4VO_3 quasi-hexagonal microplates was carried out in an air atmosphere (Fig. 2b). The TG curve shows one main step corresponding to the decomposition of the NH_4VO_3 quasi-hexagonal microplates, which can be confirmed by the endothermic peak (~200 °C) of the differential scanning calorimetry

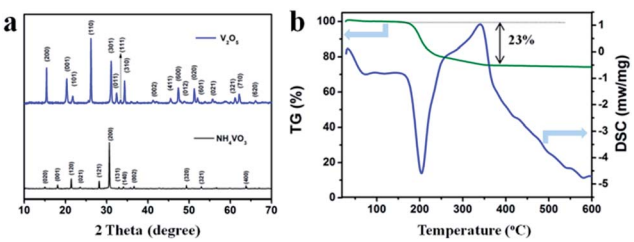

Fig. 2 (a) XRD patterns of the prepared products before and after annealing. (b) TG analysis of 3D porous V_2O_5 hierarchical plates in air.

(DSC) curve. The weight loss is 23%, and the value is close to the theoretical weight loss of the decomposition of NH_4VO_3 (22.3%); the remaining weight loss may be attributed to the decomposition of residual organics. The DSC curve also exhibits an exothermic peak at ~350 °C; it is confirmed that there is a phase transformation of V_2O_5.

Nitrogen adsorption–desorption isotherms were further measured to characterize the porous structure of the products. It is found that V_2O_5-350 has a Brurauer–Emmerr–Teller (BET) surface area of 32 $m^2\ g^{-1}$ with mesopores and macropores from 2–5 to 10–100 nm based on the Barrett–Joyner–Halenda (BJH) method (inset of Fig. 3a). The sorption isotherms of V_2O_5-350 (Fig. 3a) appear to be type IV curves, with H3 hysteresis loops that can be linked to slit-shaped pores. Fig. 3b shows that with increasing calcination temperature, the average pore diameter of the V_2O_5 sample increases, whereas the BET surface area and pore volume of the V_2O_5 sample decreases, suggesting that the porous structure of the products was changed (Fig. S6 and S7†). The BET surface area of the V_2O_5 sample annealed at 600 °C decreases to ~5 $m^2\ g^{-1}$, and the porous structure does not exist according to the low BET surface area and unavailable pore size data. We also annealed the bulk NH_4VO_3 at 350 °C (Fig. S8†), whose BET surface area (21 $m^2\ g^{-1}$) and pore volume (0.15 $cm^3\ g^{-1}$) are lower than the as-synthesized porous V_2O_5 microplates calcined at the same temperature.

Coin cells with metallic lithium as the anode were assembled to investigate the electrochemical performance of the 3D porous V_2O_5 hierarchical microplate cathodes. Cyclic voltammogram (CV) of the porous V_2O_5 microplates was measured at a scan rate of 0.1 mV s^{-1} in the potential range from 2.4 to 4.0 V (Fig. 4a). The cathodic and anodic peaks are ascribed to the lithium ion insertion and extraction, respectively. Two main cathodic peaks appear at potentials of 3.30 and 3.08 V, corresponding to the phase transformations from α-V_2O_5 to ε-$Li_{0.5}V_2O_5$ and δ-LiV_2O_5, the processes of which are expressed in eqn (5) and (6), respectively.[40,43]

$$V_2O_5 + 0.5Li^+ + 0.5e^- = \varepsilon\text{-}Li_{0.5}V_2O_5 \quad (5)$$

$$\varepsilon\text{-}Li_{0.5}V_2O_5 + 0.5Li^+ + 0.5e^- = \delta\text{-}LiV_2O_5 \quad (6)$$

In the subsequent scans, the shapes of the curves are almost identical, which indicates a good reversibility of the lithium insertion process. Fig. 4b displays the discharge–charge curves of the V_2O_5 cathodes at different cycles. The result shows that the discharge–charge curves are almost superposed over 10 cycles. Two voltage plateaus are clearly observed which is quite consistent with the CV curves. The cycling performance was further evaluated by galvanostatic discharge–charge testing. As shown in Fig. 4c, the initial discharge capacity of the 3D porous V_2O_5 hierarchical microplate cathode is 146 mA h g^{-1} at 100 mA g^{-1}, very close to the theoretical value of 147 mA h g^{-1} for the formation of δ-LiV_2O_5. After 50 cycles, their discharge capacities remain at 137 mA h g^{-1}, corresponding to 93.8% of the initial capacity. Over the entire cycles, the coulombic efficiency maintains at a high level of more than 99%, demonstrating a good reversibility between the charge and discharge processes.

To evaluate the rate capability, the 3D porous V_2O_5 hierarchical microplate cathode was cycled at various rates, ranging from 50 to 2000 mA g^{-1} (Fig. 4d). As the rate increases from 50 to 2000 mA g^{-1}, the discharge capacity of the cathodes decreases gradually from 147 to 112 mA h g^{-1}. After the high rate measurement, when the rate is reduced back to 50 mA g^{-1}, a discharge capacity of 139 mA h g^{-1} can be recovered. It is obvious that the rate performance of V_2O_5-350 is better than those of the samples annealed at 450 (V_2O_5-450) and 600 °C (V_2O_5-600). Moreover, the cycling performance of the 3D porous V_2O_5 hierarchical microplates cathodes at high rates of 1000 mA g^{-1} and 2000 mA g^{-1} are shown in Fig. 4e. The initial specific discharge capacities are 130 and 110 mA h g^{-1} at the rates of 1000 and 2000 mA g^{-1}, respectively. Remarkably, their capacities are retained at 123 and 108 mA h g^{-1} after 100 cycles, corresponding to 94.6% and 98.2% of their initial capacity, respectively. In order to investigate the influence of the porous structure on the electrochemical performance of V_2O_5, electrochemical characterizations of the bulk V_2O_5 powders were also measured (Fig. S9 and S10†), indicating 3D porous architecture improves the electrochemical performance of V2O5 dramatically. The electrochemical performance of the 3D porous V_2O_5 hierarchical microplates is good compared to those of many reported V_2O_5 electrodes, in terms of a high-rate capability and cycling performance (Table S1†). The electrochemical impedance spectra (EIS) were used to provide further insights (Fig. S11†). The Nyquist plots indicate that the charge transfer resistance (Rct) of V_2O_5-350 with a higher BET surface area is much lower than those of the other two cathodes. The reason for that should be the porous structure with larger surface area increases the contact area between the active sites and electrolytes, and shortens diffusion distance for the Li^+ ions, which leads to rapid ion diffusion and an efficient charge transfer.[44] As a device that delivers high power, the Joule effect must be considered since large amounts of heat can be generated during the charge–discharge process at high power.[45] Therefore, it is crucial to study the temperature-dependent performance. Fig. 4f clearly shows that with an increase of the cycle number, the capacities at 1000 mA g^{-1} tend to increase both at 40 and 60 °C. The gradual improvement of capacity suggests the gradual penetration of the electrolyte into the particles' interior[46] and that the electrochemical kinetics are promoted gradually during

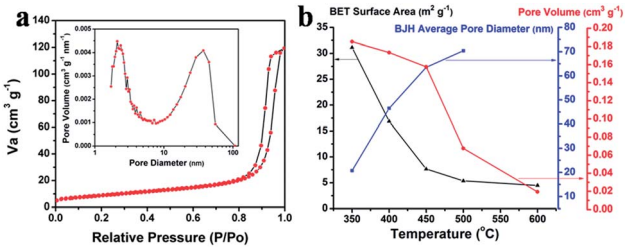

Fig. 3 (a) Nitrogen adsorption–desorption isotherms of V_2O_5-350 and corresponding pore size distribution (inset). (b) BET surface area distribution, average pore diameter and pore volume of V_2O_5 samples with different calcination temperatures.

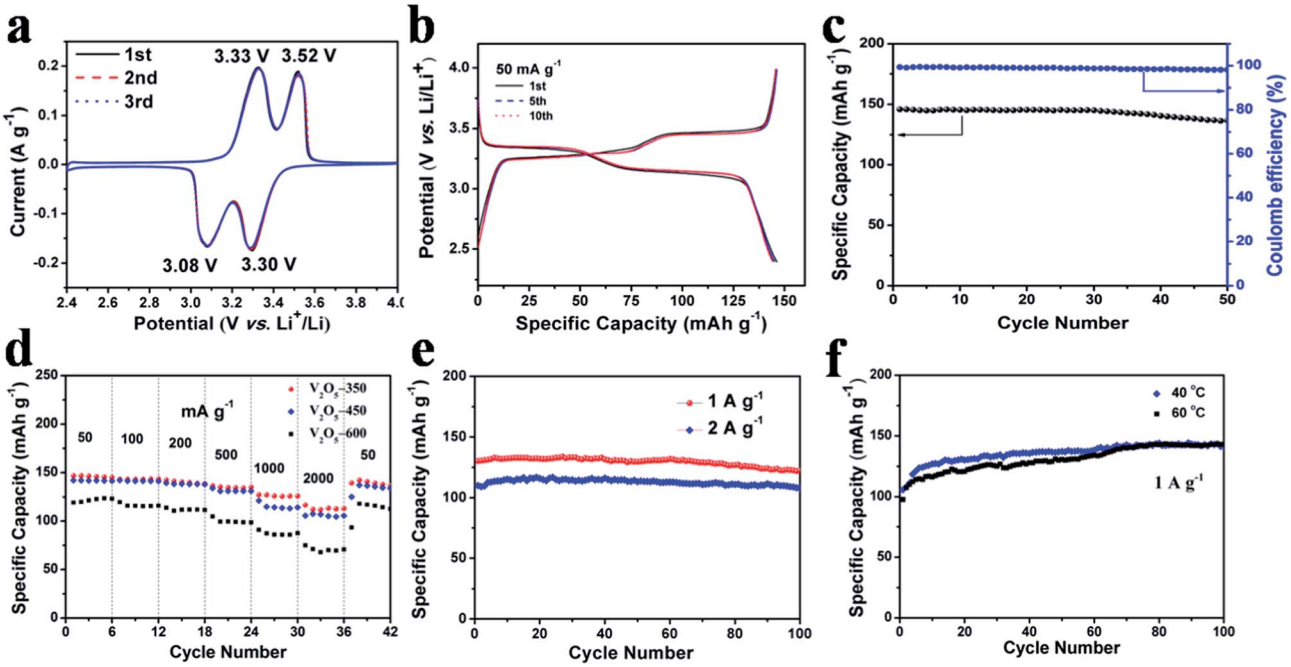

Fig. 4 (a) Cyclic voltammograms at a scan rate of 0.1 mV s^{-1} of V_2O_5-350; (b) discharge–charge curves of the first, fifth and tenth cycles at 50 mA g^{-1} of V_2O_5-350; (c) cycling performance at the current density of 100 mA g^{-1} of V_2O_5-350; (d) the rate performance of porous V_2O_5 microplates annealed at different temperatures; (e) cycling performance at high rates of 1 A g^{-1} and 2 A g^{-1} of V_2O_5-350; (f) cycling performance at a current density of 1 A g^{-1} measurement at 40 and 60 °C of V_2O_5-350.

the temperature-rise process of the cells as measured.[47] Significantly, their capacities are 141 and 143 mA h g^{-1} after 100 cycles, respectively, which are higher than those measured at room-temperature. It demonstrates that the porous V_2O_5 hierarchical microplates cathode shows a high rate capacity.

The improved rate capability and cycling stability are attributed to the interesting 3D porous structure. More specifically, the porous structure would facilitate electrolyte penetration and increase the contact area between the electrode material and the electrolyte.[48] The nanosized V_2O_5 subunits with many spaces between each other have an increased portion of exposed surfaces, which ensures a high utilization of the electrode materials and provides more electrochemically active sites for Li^+ to accesses, thus a high capacity is achieved.[49] Moreover, the porous structure might be also an advantage to accommodate the volume variations during the Li^+ ions intercalation and deintercalation.[50] Finally, the nanosized building blocks reduce the distance for the Li^+ ions' diffusion and the electron transport.[50,51] In brief, the porous structure is beneficial to the improved cycling stability and excellent rate capability of the 3D porous V_2O_5 hierarchical microplates.

Conclusions

A facile top-down fabrication approach has been developed to prepare 3D porous V_2O_5 hierarchical quasi-hexagonal microplates, *via* a one-step thermal decomposition of NH_4VO_3 microplates. The as-synthesized V_2O_5 microplates are composed of well-defined nanosized subunits, forming a highly porous hierarchical structure which gives rise to a high surface area (32 m^2 g^{-1}). When evaluated as a cathode for LBs, the V_2O_5 microplates display relatively stable capacity retention (capacity retention reaches up to 98.2% after 100 cycles). They also show excellent rate capability, with a capacity of 110 mA h g^{-1} at 2000 mA g^{-1}. The excellent electrochemical performance suggests that the unique porous V_2O_5 hierarchical microplates are a promising cathode material for LBs' applications. This one-step thermal conversion of NH_4VO_3 into porous structures can further be applied to converting ammonium salt into such porous structures. Meanwhile, this effective top-down strategy can be extended to fabricate other micro/nano materials with unique structures which have advanced electrochemical properties.

Acknowledgements

This work was supported by the National Basic Research Program of China (2013CB934103, 2012CB933003), the National Natural Science Foundation of China (51072153, 51272197), the Program for New Century Excellent Talents in University (NCET-10-0661) and the Fundamental Research Funds for the Central Universities (2013-VII-028). Thanks to Prof. C. M. Lieber of Harvard University, Prof. Dongyuan Zhao of Fundan University and Dr Jun Liu of Pacific Northwest National Laboratory for strong support and stimulating discussions.

Notes and references

1 K. T. Nam, D. W. Kim, P. J. Yoo, C. Y. Chiang, N. Meethong, P. T. Hammond, Y. M. Chiang and A. M. Belcher, *Science*, 2006, **312**, 885.

2 B. Kang and G. Cede, *Nature*, 2009, **458**, 190.
3 (*a*) M. Y. Ge, J. P. Rong, X. Fang and C. W. Zhou, *Nano Lett.*, 2012, **12**, 2318; (*b*) N. Mahmood, C. Z. Zhang and Y. L. Hou, *Small*, 2013, **9**, 1321.
4 H. Li, Z. X. Wang, L. Q. Chen and X. J. Huang, *Adv. Mater.*, 2009, **21**, 4593.
5 A. S. Arico, P. G. Bruce, B. Scrosati, J. M. Tarascon and W. V. Schalkwijk, *Nat. Mater.*, 2005, **4**, 366.
6 N. S. Choi, Y. Yao, Y. Cui and J. Cho, *J. Mater. Chem.*, 2011, **21**, 9825.
7 J. M. Tarascon and M. Armand, *Nature*, 2001, **414**, 359.
8 (*a*) M. Armand and J. M. Tarascon, *Nature*, 2008, **451**, 652; (*b*) J. P. Liu, J. Jiang, C. W. Cheng, H. X. Li, J. X. Zhang, H. Gong and H. J. Fan, *Adv. Mater.*, 2011, **23**, 2076.
9 J. B. Goodenough and Y. Kim, *Chem. Mater.*, 2009, **22**, 587.
10 C. K. Chan, H. L. Peng, G. Liu, K. McIlwrath, X. F. Zhang, R. A. Huggins and Y. Cui, *Nat. Nanotechnol.*, 2008, **3**, 31.
11 M. S. Whittingham, *Chem. Rev.*, 2004, **104**, 4271.
12 M. V. Reddy, G. V. Subba Rao and B. V. R. Chowdari, *Chem. Rev.*, 2013, **113**, 5364.
13 S. Q. Wang, S. R. Li, Y. Sun, X. Y. Feng and C. H. Chen, *Energy Environ. Sci.*, 2011, **4**, 2854.
14 Q. T. Qu, Y. S. Zhu, X. W. Gao and Y. P. Wu, *Adv. Energy Mater.*, 2012, **2**, 950.
15 S. Zhou, X. G. Yang, Y. J. Lin, J. Xie and D. W. Wang, *ACS Nano*, 2012, **6**, 919.
16 Y. Wang and G. Z. Cao, *Adv. Mater.*, 2008, **20**, 2251.
17 T. Y. Zhai, H. M. Liu, H. Q. Li, X. S. Fang, M. Y. Liao, L. Li, H. S. Zhou, Y. Koide, Y. Bando and D. Golberg, *Adv. Mater.*, 2010, **22**, 2547.
18 M. S. Whittinham, *J. Electrochem. Soc.*, 1976, **123**, 315.
19 E. Hosono, T. Kudo, I. Honma, H. Matsuda and H. S. Zhou, *Nano Lett.*, 2009, **9**, 1045.
20 A. R. Armstrong and P. G. Bruce, *Nature*, 1996, **381**, 499.
21 C. Ban, N. A. Chernova and M. S. Whittingham, *Electrochem. Commun.*, 2009, **11**, 522.
22 J. Muster, G. T. Kim, V. Krstic, J. G. Park, Y. W. Park, S. Roth and M. Burghard, *Adv. Mater.*, 2000, **12**, 420.
23 T. Watanabe, Y. Ikeda, T. Ono, M. Hibino, M. Hosoda, K. Sakai and T. Kudo, *Solid State Ionics*, 2002, **151**, 313.
24 A. M. Cao, J. S. Hu, H. P. Liang and L. J. Wan, *Angew. Chem., Int. Ed.*, 2005, **44**, 4391.
25 C. F. Zhang, Z. X. Chen, Z. P. Guo and X. W. Lou, *Energy Environ. Sci.*, 2013, **6**, 974.
26 L. Q. Mai, Y. J. Dong, L. Xu and C. H. Han, *Nano Lett.*, 2010, **10**, 4273.
27 T. Y. Zhai, H. M. Liu, H. Q. Li, X. S. Fang, M. Y. Liao, H. S. Zhou, Y. Koide, Y. Bando and D. Golberg, *Adv. Mater.*, 2010, **22**, 2547.
28 (*a*) Y. Wang, K. Takahashi, K. H. Lee and G. Z. Cao, *Adv. Funct. Mater.*, 2006, **16**, 1133; (*b*) S. Q. Wang, Z. D. Lu, D. Wang, C. G. Li, C. H. Chen and Y. D. Yin, *J. Mater. Chem.*, 2011, **21**, 6365; (*c*) C. K. Chan, H. L. Peng, R. D. Twesten, K. Jarausch, X. F. Zhang and Y. Cui, *Nano Lett.*, 2007, **7**, 490.
29 Y. W. Li, J. H. Yao, E. Uchaker, J. W. Yang, Y. X. Huang, M. Zhang and G. Z. Cao, *Adv. Energy Mater.*, 2013, **3**, 1171.
30 A. Q. Pan, H. B. Wu, L. Yu and X. W. Lou, *Angew. Chem., Int. Ed.*, 2013, **125**, 2282.
31 Y. G. Guo, J. S. Hu and L. J. Wan, *Adv. Mater.*, 2008, **20**, 2878.
32 (*a*) H. Liu, D. Su, R. Zhou, B. Sun, G. Wang and S. Z. Qiao, *Adv. Energy Mater.*, 2012, **2**, 970; (*b*) H. Liu, X. Du, X. Xing, G. Wang and S. Z. Qiao, *Chem. Commun.*, 2012, **48**, 865; (*c*) H. Liu, D. Su, G. Wang and S. Z. Qiao, *J. Mater. Chem.*, 2012, **22**, 17437.
33 Y. Q. Qiao, J. P. Tu, X. L. Wang, D. Zhang, J. Y. Xiang, Y. J. Mai and C. D. Gu, *J. Power Sources*, 2011, **196**, 7715.
34 Q. T. Qu, L. J. Fu, X. Y. Zhan, D. Samuelis, J. Maier, L. Li, S. Tian, Z. H. Li and Y. P. Wu, *Energy Environ. Sci.*, 2011, **4**, 3985.
35 (*a*) J. Y. Xiang, X. L. Wang, J. Zhong, D. Zhang and J. P. Tu, *J. Power Sources*, 2011, **196**, 379; (*b*) F. Yu, J. J. Zhang, Y. F. Yang and G. Z. Song, *J. Mater. Chem.*, 2009, **19**, 9121.
36 (*a*) Y. L. Zhao, L. Xu, L. Q. Mai, C. H. Han, Q. Y. An, X. Xu, X. Liu and Q. J. Zhang, *Proc. Natl. Acad. Sci. U. S. A.*, 2012, **109**, 19569; (*b*) L. Q. Mai, F. Yang, Y. L. Zhao, X. Xu, L. Xu and Y. Z. Luo, *Nat. Commun.*, 2011, **2**, 381.
37 V. Valtchev and L. Tosheva, *Chem. Rev.*, 2013, **113**, 6734.
38 X. Wang and Y. Li, *Angew. Chem., Int. Ed.*, 2002, **41**, 4790.
39 W. Lu, Y. Ding, Y. Chen, Z. L Wang and J. Fang, *J. Am. Chem. Soc.*, 2005, **127**, 10112.
40 X. F. Zhang, K. X. Wang, X. Wei and J. S. Chen, *Chem. Mater.*, 2011, **23**, 5290.
41 H. Yu, D. Wang and M. Y. Han, *J. Am. Chem. Soc.*, 2007, **129**, 233.
42 J. Liu and D. Xue, *Adv. Mater.*, 2008, **20**, 2622.
43 Q. Y. An, Q. L. Wei, L. Q. Mai, J. Y. Fei, X. Xu, Y. L. Zhao, M. Y. Yan, P. F. Zhang and S. Z. Huang, *Phys. Chem. Chem. Phys.*, 2013, **15**, 16828.
44 (*a*) B. G. Choi, S. J. Chang, Y. B. Lee, J. S. Bae, H. J. Kim and Y. S. Huh, *Nanoscale*, 2012, **4**, 5924; (*b*) Q. Qu, L. Fu, X. Zhan, D. Samuelis, J. Maier, L. Li, S. Tian, Z. Li and Y. Wu, *Energy Environ. Sci.*, 2011, **4**, 3985.
45 K. Zaghib, J. B. Goodenough, A. Mauger and C. Julien, *J. Power Sources*, 2009, **194**, 1021.
46 (*a*) R. Dominko, M. Bele, M. Gaberscek, M. Remskar, D. Hanzel, J. M. Goupil, S. Pejovnik and J. Jamnik, *J. Power Sources*, 2006, **153**, 274; (*b*) K. S. Park, S. B. Schougaard and J. B. Goodenough, *Adv. Mater.*, 2007, **19**, 848; (*c*) X. L. Wu, L. Y. Jiang, F. F. Cao, Y. G. Guo and L. J. Wan, *Adv. Mater.*, 2009, **21**, 2710; (*d*) R. Dominko, J. M. Goupil, M. Gaberscek, M. Remskar, D. Hanzel and J. Jamnik, *J. Electrochem. Soc.*, 2005, **152**, A858.
47 S. Franger, F. L. Cras, C. Bourbon and H. Rouault, *J. Power Sources*, 2003, **119**, 252.
48 N. Jayaprakash, J. Shen, S. S. Moganty, A. Corona and L. A. Archer, *Angew. Chem., Int. Ed.*, 2011, **50**, 5904.
49 A. Q. Pan, T. Zhu, H. B. Wu and X. W. Lou, *Chem. - Eur. J.*, 2013, **19**, 494.
50 D. Y. Chen, X. Mei, G. Ji, M. H. Lu, J. P. Xie, J. M. Lu and J. Y. Lee, *Angew. Chem., Int. Ed.*, 2012, **51**, 2409.
51 S. Q. Wang, Z. D. Lu, D. Wang, C. G. Li, C. H. Chen and Y. D. Yin, *J. Mater. Chem.*, 2011, **21**, 6365.

